Moisture modes with an oscillating vertical motion profile shape in steady-state weak temperature gradient simulations

Miguel Bernardez[1], **Larissa Back**[1]

[1]University of Wisconsin Madison

Key Points:

- There exists a periodic equilibrium in steady-state WTG simulations
- The oscillation is a moisture mode driven by vertical advection of moist static energy and radiation
- The periodicity is captured by a simple two-mode model of moisture and vertical motion variations

Corresponding author: Miguel Bernardez, `bernardez@wisc.edu`

Abstract

Weak Temperature Gradient (WTG) modeling using a small cloud-resolving model (CRM) admits multiple equilibria depending upon the initial model conditions. A new kind of equilibrium is presented here which undergoes a periodic and steady-state oscillation that is emergent from static boundary conditions. The periodic oscillation is shown to be a moisture mode with an oscillating vertical motion profile shape generated by the interaction between vertical motion and radiation. A simple two-mode model based on decomposing the vertical motion profile and associated radiative cooling variations can describe the oscillation.

Plain Language Summary

The weak temperature gradient approximation is an important tool used to simulate large-scale vertical motion in simplified models called cloud-resolving models using the characteristics of the environment including the sea surface temperature and air temperature. Previous research has identified two different equilibria that a weak temperature gradient simulation can settle into depending on the initial conditions. This research presents a new kind of equilibrium where the vertical motion and moisture undergo a steady state oscillation, which we call the periodic equilibrium. We show that this equilibrium can be described as a moisture mode, which is an important kind of tropical variability, and driven only by the vertical motion and radiation. We describe the oscillation and propose a simple model to describe the variability. The periodic equilibrium presented here can provide a useful tool for improving our understanding of how tropical convection evolves.

1 Introduction

The weak temperature gradient (WTG) framework is foundational to understanding the tropical atmosphere, accurate weather forecasting, and climate prediction (Charney, 1963; Sobel & Bretherton, 2000; Sobel et al., 2001; Á. F. Adames, 2022). The WTG framework is the basic assumption that horizontal temperature gradients, due to fast gravity wave redistribution, are small enough to be ignored. This causes vertical advection of dry static energy (DSE) to be the primary balance of diabatic heating. The WTG framework has been used to study a range of tropical problems, from understanding the MJO (Á. F. Adames & Kim, 2016; Wang et al., 2016; Sentić & Sessions, 2017), to understanding the interactions between moist convection and the large-scale environment (Sobel & Bretherton, 2000; Neogi & Singh, 2022; Singh & Neogi, 2022), as well as the evolution of slower developing systems like some tropical waves (Á. F. Adames, 2022). Perhaps the most practically useful implementation of the WTG framework is as a parameterization of large-scale vertical motion in cloud-resolving models as in Raymond and Zeng (2005).

Models that use a WTG parameterization display an important behavior, called multiple equilibria, where the model will enter either a dry or moist equilibrium depending on the initial conditions of the model (Sobel et al., 2007; Sessions et al., 2010; Wong & Kuang, 2023). The moist equilibrium, as the name would suggest, is characterized by high column water vapor, consistent precipitation, and ascending vertical motion. The dry equilibrium, on the other hand, is characterized by low column moisture, a lack of rain, and general descending motion. The dry and moist equilibria are thought to correspond to the dry and moist areas that arise due to convective aggregation (Raymond et al., 2009). Generally, the dry equilibrium is discarded and avoided because research is primarily interested in moist convection and the dry equilibrium can become non-physically dry. For example, realistic values for the dry region of the atmosphere are 20-40 mm of column water vapor (CWV) (Mapes et al., 2018) and values around 10 mm are seen rarely in the far tropics (Mapes et al., 2018). The dry equilibrium simulations we generated for

this research have values around 6 mm of CWV, so it is generally good practice to disregard and avoid the dry equilibrium.

A model will enter the moist or dry equilibrium depending on the model's reaction to the convective forcing and whether there will be an export or import of moist static energy, or moist entropy, as the simulation develops. A simulation will enter and stay in the moist equilibrium if it is able to import enough moisture and moist static energy to sustain deep convection. The prevalence of multiple equilibria and whether or not a simulation will enter a particular equilibrium depends on the specifics of the model. For instance, the choice of radiation and horizontal moisture transport parameterizations are important for the existence of multiple equilibria (Sessions et al., 2015, 2016). We also know that whether a particular simulation will enter the dry equilibrium is impacted by the initial conditions of the model; sometimes by increasing the initial moisture, we can move a model into the moist equilibrium (Sessions et al., 2010, 2015; Wang et al., 2016).

When performing realistic simulations, we have avoided the dry equilibrium by nudging the model towards the moist equilibrium by increasing moisture. This is precisely what we were attempting when we discovered a new twist in the story of WTG multiple equilibria, a new kind of equilibrium state where the moisture, precipitation and vertical motion display steady state oscillatory behavior.

In recent SWTG simulations of climatological vertical motion profile shape, Bernardez and Back (2024) had unpublished early simulations that entered into the dry equilibrium. They modified the initial moisture profile hoping to simulate a moist equilibrium state and the model entered into a new kind of equilibrium where the model state, primarily the moisture and vertical motion, underwent a steady-state oscillation of convective amplification and decay (figure 1). These were simulations that had constant imposed horizontal advection and no time-dependence in the boundary conditions to drive the variability. The oscillation appears as an emergent phenomenon from the internal interactions of the model.

This oscillation has now been seen in other research using WTG simulations. Raymond et al. (2024) found the oscillation during an investigation of field campaign observations and described the oscillation in terms of the rains versus showers schema introduced by Ramage (1971). Wong and Kuang (2023) reported oscillatory behavior during their investigation of different WTG implementations, although they did not discuss the oscillations in detail. The periodic equilibrium was also seen by Dr. Tristan Abbott confirmed through personal correspondence. We shall discuss the differences in model setup and description of the oscillation between the present research and that of Raymond et al. (2024) further in the discussion.

Through the rest of the paper, we will go over the model and simulations that produced the periodic equilibrium. Afterward, we will discuss the oscillation and its features. Next, we will show that the simulations are a moisture mode where vertical advection drives the oscillations and go over a two-mode model that can capture the oscillation. Finally, we will discuss what our results mean to our understanding of vertical motion in the tropics.

2 Weak Temperature Gradient model

We initially discovered the periodic equilibrium during the preliminary work of Bernardez and Back (2024), which used the weather research and forecasting model (WRF) (version 3.5.1) (Skamarock et al., 2008) as the small scale cloud-resolving model (CRM) and the spectral WTG parameterization from Wang et al. (2016), as the specific WTG parameterization. We used a timescale for the first WTG mode of one hour and calculate the first 10 modes of the spectral decomposition. The modes are calculated from the stability as in Wang et al. (2016) using the reanalysis data as we describe later in this sec-

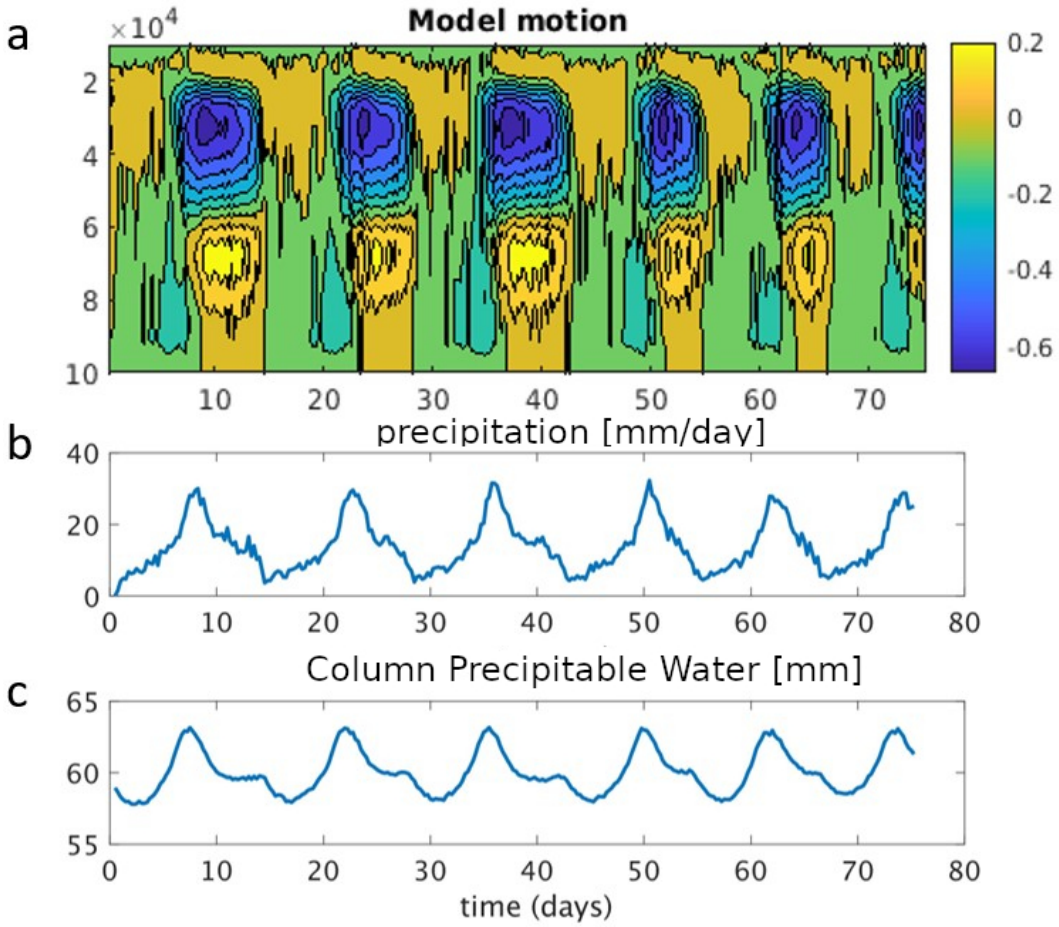

Figure 1. Time series of periodic equilibrium found in spectral weak temperature gradient simulations. Panel (a) shows the contours of the SWTG vertical velocity produced by the model in units of [pa/s] with a contour interval of .01 [pa/s], panel (b) the precipitation produced by the model, and panel (c) the time series of column water vapor (CWV).

tion. The boundaries of the model are comprised of a constant single value of SST for the lower boundary condition, doubly periodic lateral boundaries with an imposed horizontal moisture advection for the horizontal, and a momentum damping scheme that acted as the upper boundary (Klemp et al., 2008). The simulation has a domain size of 64x64x23 km, with a horizontal grid size of 1 km and a vertical grid size set such that there are 60 stretched levels with 10 in the lowest kilometer of the atmosphere.

The model domain has its horizontal winds relaxed back to the original profile with a relaxation rate of one hour. We used the Morrison two-moment scheme to parameterize the microphysics(Morrison et al., 2009). The RRTMG long-wave scheme and the Goddard short-wave scheme parameterize the radiation (Iacono et al., 2008; Chou & Suarez, 1999; Matsui et al., 2007; Shi et al., 2010). The solar insolation is set to a constant value of $370 W/m^2$ so that we do not have a diurnal cycle. We parameterize subgrid scale eddies using the three-dimensional Smagorinsky first-order closure scheme and an implicit vertical diffusion scheme is used to ensure numerical conservation of moisture. Everything else that we have not mentioned is kept the same as Bernardez and Back (2024).

The data that we used is sourced from the ERA-5 reanalysis of a region in the Central-Eastern Pacific (Hersbach et al., 2019a). We take the surface temperature, SST, and moisture values along with the profiles of temperature, wind, and moisture. The temperature, SST, and horizontal wind profiles go directly into initializing the model and maintaining the model state. The moisture profiles are used to calculate the horizontal moisture advection that we impose. We construct our data by averaging daily data from 2008 through 2019 in the region bounded by 7.5-10°N 120-140°E.

SWTG parameterizes the effects of domain-scale vertical motion that acts to relax the domain mean temperature profile towards a specific reference profile. We choose not to directly use the reanalysis temperature profile because of the differences between real-world physics and model representation, so we obtain a temperature profile consistent with the model. We use an equilibrium model state known, in the literature, as either radiative-convective dynamic equilibrium (RCDE) (Singh et al., 2019) or radiative-convective-advective equilibrium (RCAE) Romps (2021), but which we call the driven equilibrium (DE).

We create the DE simulations by imposing the large-scale tendencies in moisture and temperature associated with the vertical motion profile that we wish to emulate and allowing the model to evolve to equilibrium. The horizontal advection is also imposed for these simulations as well as in the SWTG simulations. Because we assume there is a finite relaxation timescale, the mean temperature profile of the DE simulation still has a temperature anomaly associated with the active convection relative to the largescale background temperature that we wish to emulate (See Bernardez and Back (2024) for a complete description). We correct the temperature profile for this anomaly and utilize the corrected DE temperature profile as the reference profile for calculating the SWTG vertical velocity.

We initialized a simulation (not the one utilized in this paper) with the reference temperature profile and an initial moisture profile that is taken from the DE simulation. The simulation was initialized with the wind profile, SST, and imposed horizontal moisture advection from reanalysis as well (see (Bernardez & Back, 2024)). This first simulation went to the dry equilibrium and, to nudge the model towards the moist equilibrium, we set the moisture profile so that it had a uniform relative humidity of 85 % and ran the model again. This simulation entered into the new equilibrium where the model state undergoes a steady-state periodic oscillation, which we describe in the next section.

3 The Periodic Equilibrium: a Moisture Mode

We were successfully able to force the model to leave the dry equilibrium by setting the moisture to 85 % RH through the depth of the column, at which point the simulation enters a new kind of equilibrium where the moisture and vertical motion fields show a distinct steady-state oscillation. The basic features of the oscillation are shown in figure 1 using the WTG vertical motion, the column-integrated water vapor (CWV), and the precipitation reported by the model. The simulation and oscillation begin with a period of shallow bottom-heavy vertical motion which acts to slowly decrease the CWV while the precipitation slowly increases. The precipitation and moisture then rapidly increase as the vertical motion becomes deeper and extends through the depth of the column. After precipitation and CWV peak, the vertical motion becomes stratiform and both the precipitation and CWV start decreasing. The stratiform vertical motion ends when the moisture and precipitation reach a minimum and the cycle is restarted. The period of the oscillation is approximately 14 days, although the lack of a diurnal cycle makes comparison to days in the real atmosphere somewhat dubious.

Upon first discovering the new equilibrium, we tested several different aspects of the model, to figure out how, why, and when the periodic equilibrium appears. We only obtained a periodic oscillation when using an interactive radiation scheme and imposed horizontal moisture advection. Doubling or halving the characteristic WTG relaxation time-scale doubled/halved the period of the oscillation. Changing the SST, temperature, moisture, or wind profiles would sometimes excite the periodic equilibrium. However, we were not able to determine a perceptible pattern from the basic tests that we conducted, so we moved onto studying the behavior of the oscillation. All of the periodic equilibrium simulations are consistent with the results that we report here, so we only show the results from the first simulation which displayed the oscillatory behavior.

The oscillations have many of the markers of a moisture mode, which is a dynamical mode that acts through the prognostic moisture (Fuchs & Raymond, 2007; Sobel & Maloney, 2012, 2013; Á. F. Adames et al., 2019; Ahmed et al., 2021). Recent research has started to reveal the importance of moisture modes to the tropical atmosphere and the implication that they are emergent in SWTG models is attractive. Understanding the periodic equilibrium could provide a crucial tool to understand and correctly parameterize moisture mode behavior.

Ahmed et al. (2021), building off of work by Á. F. Adames et al. (2019), established three criteria for determining a moisture mode, which we show our simulation satisfies in figure (2). Each dot is a model output time step and the dots are 6 hours apart in model time. The criteria are (a) a strong correlation between precipitation and the total column water, (b) a leading order WTG balance in the DSE budget, and (c) variations in MSE anomalies are dominated by moisture anomalies.

The color of each dot corresponds to the top-heaviness angle (Bernardez & Back, 2024), which is a measure of the shape of the vertical motion profile and differentiates ascent versus descent and top-heavy versus bottom-heavy. The top-heaviness angle is calculated by projecting the vertical motion onto two structure functions, then taking the ratio of the amplitudes of the two structure functions, and finally taking the arctangent to get an angle. The two structure functions are the first two empirical orthogonal functions from a principal component analysis of vertical motion as a function of pressure. We use ERA5 daily vertical motion profiles over maritime regions from 1979 to 2019 to calculate these structure functions. Details of how the top-heaviness angle is calculated are found in Bernardez and Back (2024). The top-heaviness angle is used here only for visual clarity.

The first criterion, seen in panel (a), is a strong correlation between the precipitation and column water vapor anomaly. There is a broadly linear relationship between

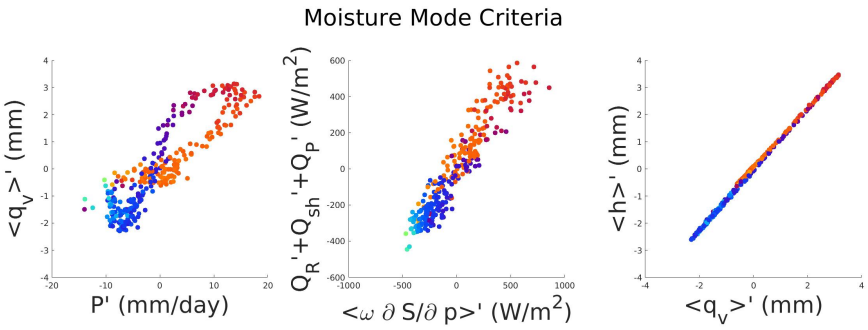

Figure 2. Moisture mode criteria are satisfied for the periodic equilibrium shown in figure (1). a) The relationship between the column water vapor (CWV) anomaly and the precipitation anomaly, b) the relationship between apparent heating and vertical advection of DSE, and c) the relationship between column MSE anomalies and column moisture anomalies. Each point is colored based on the vertical motion profile shape called the top-heaviness angle, following Bernardez and Back (2024), for visual clarity.

the two and a clear hysteresis. The section of the period with the greater slope occurs during the amplification phase and the section with the lesser slope occurs during the contraction phase.

The second criterion is a leading order WTG balance in the dry static energy (DSE) budget:

$$\omega \frac{\partial s}{\partial p} = Q_R + Q_p + Q_{sh}. \tag{1}$$

Here $s = c_p T + gz$ is the DSE, ω is the pressure velocity, Q_R is the column radiative heating, Q_P is heating from condensation, and Q_{sh} is the surface sensible heat flux (panel b). This criterion is forced by the SWTG parameterization and the nature of the model, and the figure confirms the balance.

The final criterion is for variations in the moist static energy (MSE), which is the sum of the DSE and the latent heat $h = s + l_v q_v$, to be dominated by moisture variations (panel c). This criterion is also enforced partially by the SWTG parameterization and would be enforced fully using a strict implementation of WTG.

With all three criteria for a moisture mode satisfied by the periodic equilibrium, we can call it a vertical motion moisture mode. The variations in this vertical motion moisture mode are driven by differences in the vertical motion profile shape.

The column MSE budget is a useful tool for studying moisture modes because of its relationship to moisture and precipitation. The equation for the column energy budget is:

$$\frac{\partial \langle h \rangle}{\partial t} = \langle \omega \frac{\partial h}{\partial p} \rangle + Q_{hadv} + Q_{rad} + Q_{lh} \tag{2}$$

Here h is the MSE, defined as $h = c_p T + gz + L_v q_v$, where T is the temperature, z is the height, q_v is the specific humidity, and c_p, g, and L_v are the constants of specific heat of air, gravitational acceleration, and latent heat of vaporization. Q_{hadv} is the column horizontal MSE advection, which in our case is the imposed horizontal moisture advection that is constant in time, and Q_{lh} is the surface latent heat flux. The $\langle\rangle$ represents a mass-weighted integral over the depth of the troposphere. The surface sensible heat flux is small enough in our cases that we ignore it.

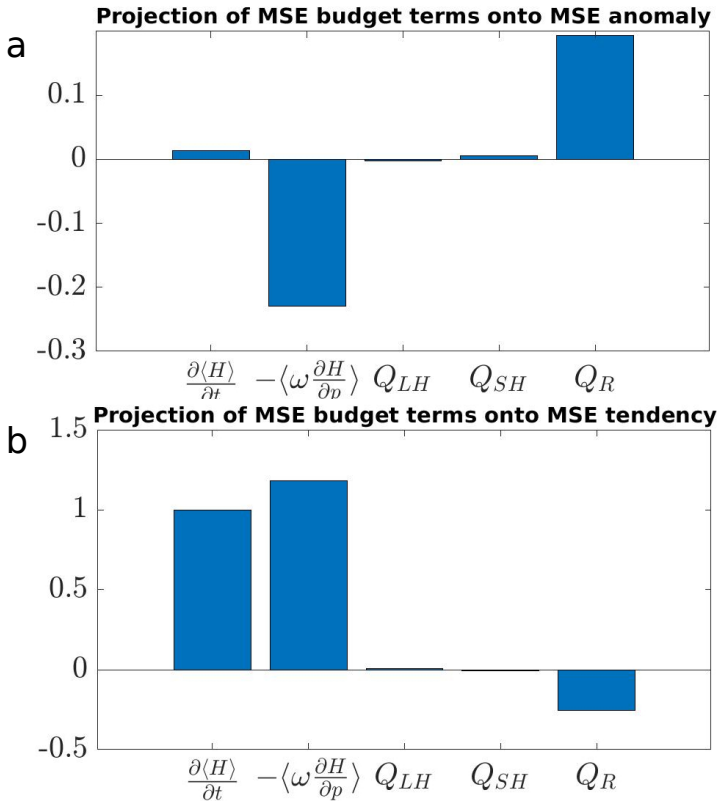

Figure 3. Projection of MSE budget terms onto the column MSE anomaly in the periodic equilibrium shown in figure (1) (a) and the column MSE tendency (b), which shows the relative contribution of each term to the maintenance of the moisture mode (a) and propagation of the moisture mode (b).

A prevalent way of investigating moisture modes is to use the MSE budget to investigate how each MSE budget term contributes to the amplitude and the period of the wave (Andersen & Kuang, 2012; Á. F. Adames, 2017; A. F. Adames & Maloney, 2021; Mayta et al., 2022). The time series of the column MSE anomaly measures the amplitude of the wave and we can measure how each term in the MSE budget contributes to the maintenance of the amplitude by projecting the time-series of each budget term onto the column MSE anomalies (figure 3 a), given by:

$$M_x = \frac{\|x \cdot \langle h\rangle'\|}{\|\langle h\rangle'^2\|}. \tag{3}$$

Here M_x is the maintenance contributed by x, because it shows what contributes to maintaining the amplitude of the wave, and $||y||$ is the integral over the time-series.

The column MSE anomaly projection, shown in figure (3 a), shows how much each term contributes to amplifying or weakening the moisture mode oscillation. The two most important terms in the energy budget are radiation and MSE advection, which is essentially the combination of moisture and vertical motion variability. The radiative cooling contributes to amplifying the wave and increasing the variations in column MSE over time while the MSE advection contributes to damping the wave. It is only their balance that leads to the steady-state oscillation that we observe.

The projection of the time series of the budget terms onto the column MSE tendency gives us the propagation term:

$$P_x = \frac{\|x \cdot \langle \partial h/\partial t \rangle\|}{\|\langle \partial h/\partial t \rangle^2\|}. \tag{4}$$

The propagation shows how much each term contributes to the period of the oscillation. The contribution of the budget terms to the propagation of the moisture mode is shown in figure (3 b). We see that the most important terms are again the MSE advection and the radiation, although this time the radiation is relatively less important. The majority of the work is being done by the vertical MSE advection increasing the propagation of the wave and the radiative heating slowing it down.

Generally, vertical advection and radiation changes are coupled together in the atmosphere. They also tend to balance energetically such that their combined effect on convection is to neither amplify nor decay (Back & Bretherton, 2009a; Inoue et al., 2020). We see the same balance through the maintenance terms. We need to dig deeper to understand how the radiation and vertical advection interact to generate the moisture mode variability while still maintaining a steady-state. We do this by decomposing the vertical motion and radiation into two modes of vertical variability which explain the variance of the moisture mode the best. In the next section, we will discuss the derivation of the simplified model and go over what it tells us about the oscillation.

4 Two-Mode Framework

4.1 Vertical Advection

Two-mode models of vertical motion are common in the field in part because the vertical velocity profile variability tends to be dominated by the first two modes of variability. When principal component analysis is used to look at how vertical motion profiles vary, we find that two modes explain more than 85 % of the variance (Back et al., 2017). Utilizing the two modes, we rewrite the vertical motion as:

$$\omega(x, y, p, t) = o_1(x, y, t)\Omega_1(p) + o_2(x, y, t)\Omega_2(p) \tag{5}$$

Here o_i are the amplitudes of Ω_i, the vertical modes that are used to decompose the vertical motion. We can calculate the specific modes we use in several ways including solving the anelastic equations (Wang et al., 2016), using a Fourier transform (Herman & Raymond, 2014), or using principal component analysis (PCA) to find the vertical structures which explain the most variance (Back et al., 2017). We choose to use vertical modes calculated from PCA of 40-year climatology of daily maritime vertical motion data from ERA5 (Hersbach et al., 2019b). We have verified that the results of the following section were not sensitive to this choice by repeating the analysis using the vertical modes calculated using PCA of the WTG vertical motion. We apply the vertical decomposition to the vertical motion and keep only the first two modes based on the criteria of North et al. (1982).

The distinct vertical shapes of the two modes mean they interact with the MSE and DSE budgets differently. To show how this we start with the vertical advection component of column integrated MSE budget:

$$\int_{p_{surface}}^{p_{top}} \omega \frac{\partial h}{\partial p} \frac{\partial p}{g} \tag{6}$$

We next integrate by parts, apply mass continuity and assume that there is no vertical motion at the surface and top:

$$\int_{p_{surface}}^{p_{top}} \omega \frac{\partial h}{\partial p} \frac{\partial p}{g} = -\int_{p_{surface}}^{p_{top}} h \frac{\partial \omega}{\partial p} \frac{\partial p}{g} = \int_{p_{surface}}^{p_{top}} h \nabla \cdot \vec{u} \frac{\partial p}{g} \tag{7}$$

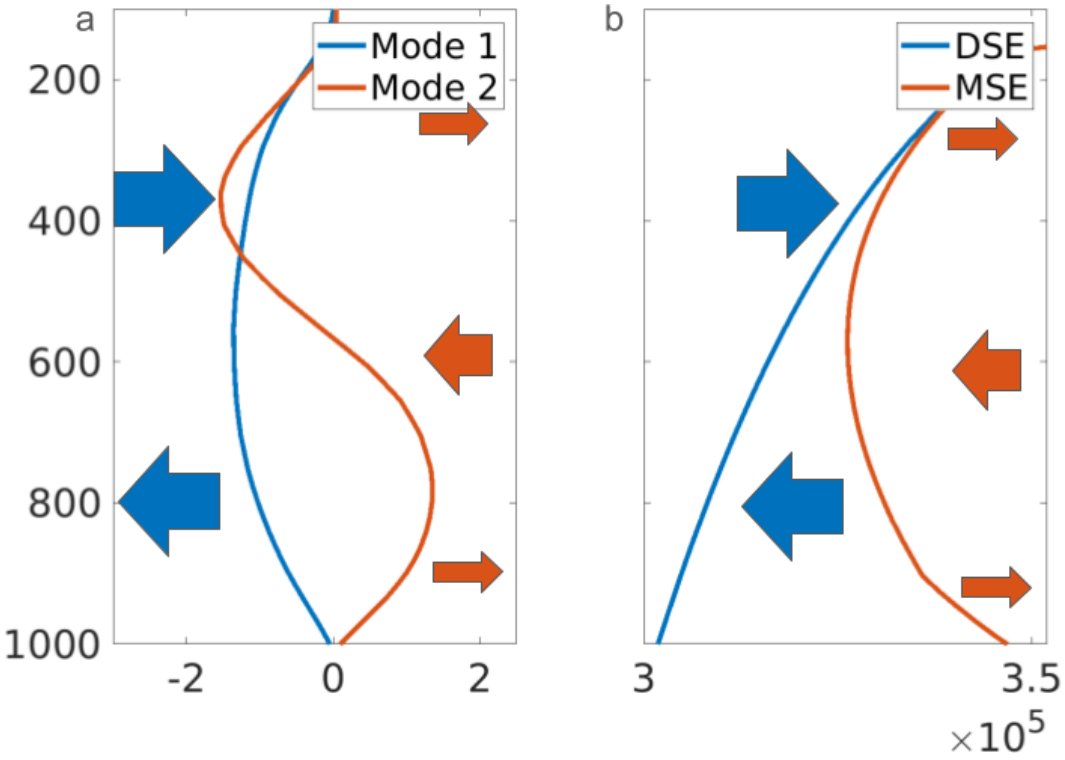

Figure 4. An illustration of the impacts of vertical motion on moist static energy and dry static energy budgets using (a) the first and second modes of vertical motion and their associated convergence along with (b) an example profile of MSE and DSE . The arrows indicate the direction of the convergence associated with the vertical motion. When they are pointed to the left energy is entering the column and when they are pointed to the right energy is leaving the column. The color of the arrow reflects the mode of vertical motion.

This shows that the column integrated vertical advection of MSE, and by extension DSE, is determined by the slope of the vertical motion profile and the profile of MSE and looks like the integrated convergence of MSE. Vertical velocity increasing with height is associated with convergence of MSE and DSE and decreasing with height is associated with divergence of MSE and DSE. A diagram of this is shown in figure (4), along with simplified profiles of DSE and MSE. The arrows indicate the circulation associated with the modes with a rightward arrow showing the divergence where the energy is leaving the column and a leftward arrow indicates convergence and energy entering the column. The arrow is colored by the vertical mode.

We can see that the first mode has a strong influence over the DSE budget due to the very different energies that it is importing versus exporting but has a much smaller impact on the MSE budget. The second mode will have very little effect on the DSE budget while having a much larger impact on the MSE budget. Based on this, we expect that the first mode should have a strong impact on the DSE budget, and thus the precipitation, but should not affect the MSE budget as much, and thus have less impact on convective amplification or decay. The second mode, on the other hand, should show little effect on the precipitation, while having a much stronger effect over convective amplification.

To confirm this, we apply the two-mode simplification to the projection of the MSE budget terms onto the MSE budget, as in figure 3, so that we can see the contribution of each mode to propagation and maintenance (figure 5 a and b). To do this we calculated the advection contributed by each mode, along with the residual, and we project those time-series onto the MSE tendency and anomaly as we did with the full vertical advection. The first panel shows how each mode's contribution to the vertical advection maintains the oscillation and it is apparent that the first mode does not have a large impact. The second panel shows the contribution of each mode to vertical advections' role in setting the period of the wave and again we see that the second mode is more important than the first mode. The oscillation variability occurs primarily in the MSE budget, which the first mode does not have much of an ability to affect, so the lack of contribution to the propagation of the vertical motion moisture mode matches the expectations we had from the simplified picture of our two modes above. Next, we apply the same decomposition to the radiation.

4.2 Radiation

Variability in radiative heating is caused primarily by moisture differences in the form of clouds, rain, and water vapor, which tends to be correlated with the vertical motion that moves the moisture around. This means that we can understand the contribution of the radiation to the two-mode model by assuming that the radiative heating variability is controlled by the vertical motion variability as Back and Bretherton (2009b) did. We do this using the following linear regression model which we solve using a least squares approach:

$$Q_{rad} = r_0 + o_1 r_1 + o_2 r_2 + \epsilon_r = r_0 + R_1 + R_2 + \epsilon_r \tag{8}$$

Where r_0 is the constant column radiative heating, and $r_{1,2}$ are the column radiative heating rate constants associated with each mode. R_1 and R_2 are the product of the constant with its corresponding mode, which gives the portion of radiative heating contributed by that mode.

The contribution of the radiation from each mode to maintenance and propagation can be seen in the middle panels of figure 5 (c,d). In short, radiative heating tries to increase the amplitude of the oscillation and both modes contribute about equally to that goal. The propagation of the oscillation by the radiation is contributed primarily by the second mode, which resists propagation, and the radiative variations associated with the first mode are not important to the propagation of the oscillation.

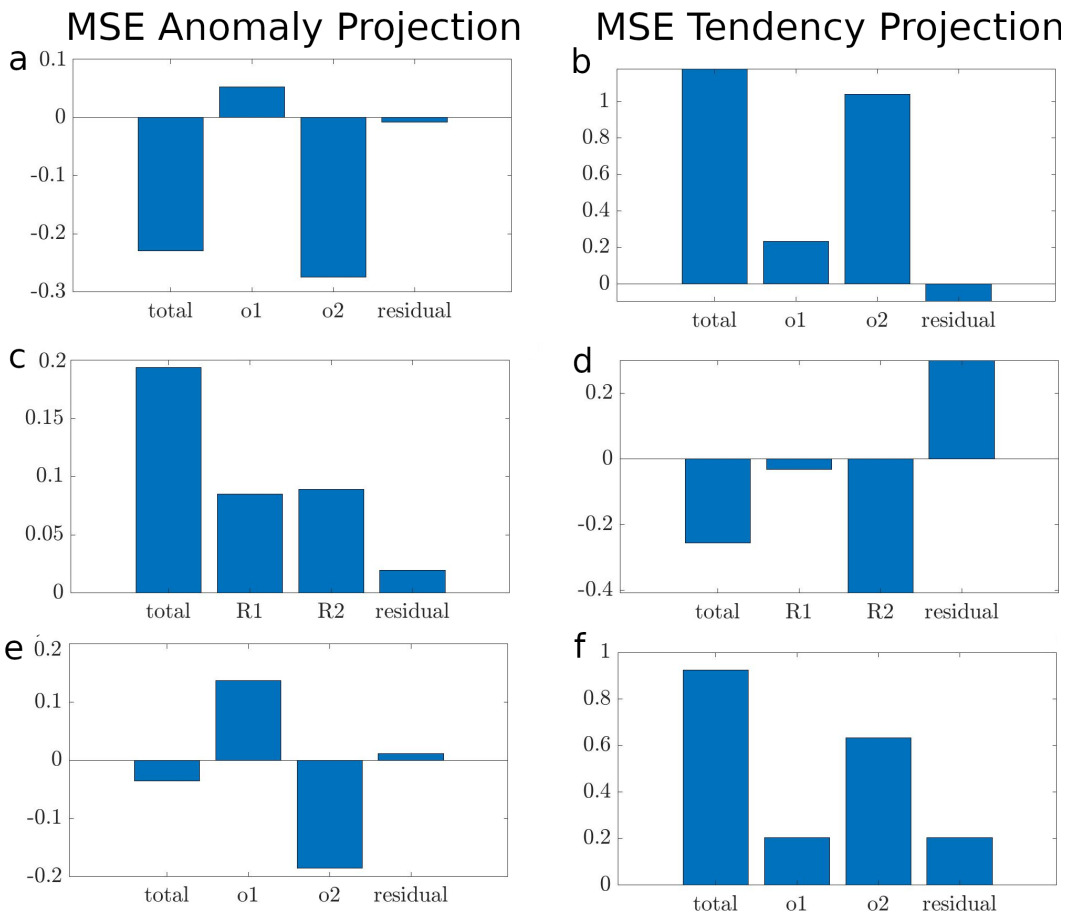

Figure 5. The contributions from each vertical mode to the column MSE budget projected onto column MSE anomaly (a,c,e) and the column MSE tendency (b,d,f), which shows the relative contribution of each term to the maintenance of the moisture mode and propagation of the moisture mode. The top panel (a,b) shows the relative contribution of the two modes to the vertical advection of MSE. The middle panels (c,d) show the relative contribution of each mode to the column radiative heating. The bottom panels (e,f) show the contribution of each mode to the combination of the MSE advection and column radiation, which means it is the top panel subtracted from the bottom panel.

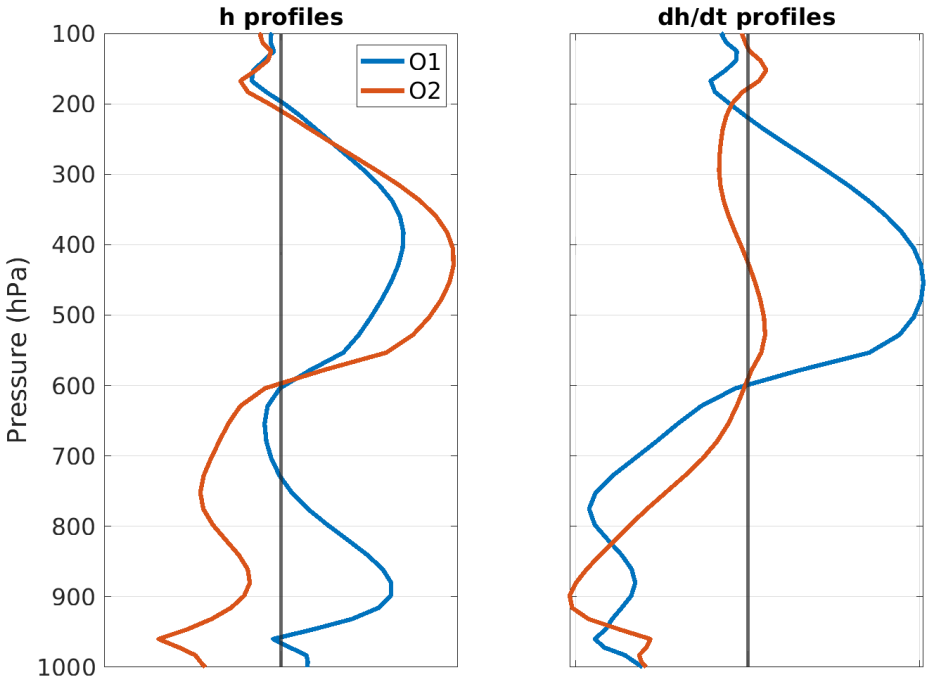

Figure 6. MSE anomalies and MSE tendency anomalies for the periodic equilibrium are projected onto each of the two vertical motion profile mode amplitudes. The first panel shows the MSE profiles that correlate with and excite the two modes (blue and orange) that we get by projecting the MSE anomalies onto each mode. The second panel shows the MSE anomaly that each of the modes tends to excite, which is given by projecting the MSE tendency onto each of the two modes.

The residual of the radiation, the part of the radiative heating that is not explained by the two-mode approximation, is also important for wave propagation. The radiation residual driving propagation is the largest effect that any of the residuals display, which indicates the two-mode model does a good job of explaining the oscillation. We now move on to understanding how the combined effects of radiation and vertical advection control the oscillation.

4.3 Combined Effects

The sum of the vertical advective and radiative effects is shown in the bottom panels of figure (5 e and f). It shows the maintenance of the oscillation is accomplished by a balance of both modes, with the first mode trying to amplify the wave and the second mode trying to reduce the wave amplitude. The first mode effect is primarily due to the radiation while the second mode effect is due mostly to the vertical advection. The propagation of the moisture mode is primarily accomplished by the second mode and within the second mode the vertical advection drives the oscillation and the radiation reduces the propagation. To summarize, the second mode is responsible for the propagation of the oscillation and the balance between the two modes is responsible for the steady-state nature of the oscillation.

The interaction between the radiation and vertical advection which leads to the oscillation is complex. However, we can simplify with more linear regression, this time focused on looking at understanding the vertical variability. We project the MSE anomalies and tendency at each height onto each of our two modes individually, shown in figure (6). These profiles are the level-by-level correlation between MSE anomaly and tendency and the time series of each mode and they represent how the MSE excites the vertical motion and how the vertical motion affects the tendency of MSE anomalies, respectively. The previous section showed that the two-mode model explains most of the contributions of both the radiation and the vertical advection, which means these correlations represent the combined effects of both the radiation and vertical advection on the MSE.

The first panel shows MSE anomaly profiles, which are the MSE anomaly profiles that tend to correlate with or excite each mode. A positive first mode, which corresponds to general ascending motion, is excited by either a lower or upper tropospheric MSE anomaly, with the lower tropospheric anomaly being more powerful in excitation. This means that the first mode is generally excited by a column relative humidity (CRH) anomaly:

$$CRH = \frac{\int_{P_{surface}}^{P_{top}} qv \partial p}{\int_{P_{surface}}^{P_{top}} qv^{\star} \partial p}.$$

Here qv is the specific humidity, $qv^{\star}$ is the saturation specific humidity.

The second mode is excited by a dipole MSE structure with a negative MSE anomaly in the lower troposphere and a positive anomaly in the upper troposphere, which tends to generate a top-heavy vertical motion profile shape. The separation point between the positive and negative lobes appears around 600 hPa or the approximate freezing level. This anomaly can be tracked by a metric we call the moisture dipole coefficient, which is defined as:

$$MDC = \frac{\int_{P_{surface}}^{P_{middle}} qv/qv^{\star} \partial p}{\int_{p_{surface}}^{P_{middle}} \partial p} - \frac{\int_{P_{middle}}^{P_{top}} qv/qv^{\star} \partial p}{\int_{P_{middle}}^{P_{top}} \partial p}.$$

The middle pressure level is set at 600 hPa. The two modes are generally excited by an MSE anomaly that is of a similar vertical shape to the vertical motion and MSE relationships. We can see the relationship between the vertical motion PCs and our two moisture metrics in figure (7). The CRH generally follows the first mode of vertical motion and the MDC generally follows the second mode with a sign change. Next, we look at how each of the modes generates MSE anomalies.

The second panel shows the projection of the MSE tendency onto each of the modes individually. The correlation between each mode and the tendency of MSE shows the MSE anomalies that each mode tends to generate. The first mode excites a dipole MSE anomaly structure, with a positive MSE anomaly in the upper troposphere and a negative MSE anomaly in the lower troposphere. The second mode tends to excite a negative MSE anomaly response in only the lower troposphere.

We can now put together the story of the oscillation through our understanding of the vertical dimension provided by figure 6. The first mode tends to correlate with a CRH anomaly and tends to excite a negative MDC anomaly. The second mode tends to correlate with a negative MDC anomaly and excite a negative CRH anomaly.

We describe the equations corresponding to this oscillation below. We start by writing down the correlations from the first panel of 6 in equation form:

$$\begin{aligned} CRH &\approx a_1 o_1 \\ MDC &\approx -a_2 o_2. \end{aligned} \tag{9}$$

The second panel gives the correlation with the tendency of MSE, and shows that the first mode correlates with an MDC anomaly tendency and the second mode correlates

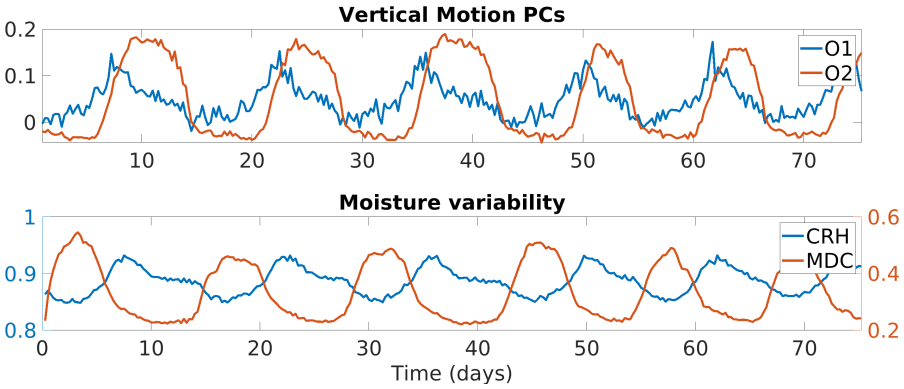

Figure 7. The upper plot shows the PCs of the first two vertical motion EOFs and the lower panel shows the CRH and MDC.

with a CRH anomaly tendency:

$$\begin{aligned} \frac{\partial CRH}{\partial t} &\approx -a_3 o_2 \\ \frac{\partial MDC}{\partial t} &\approx -a_4 o_1. \end{aligned} \tag{10}$$

Combining these with the previous set gives the series of first-order linear differential equations:

$$\begin{aligned} \frac{\partial o_1}{\partial t} &\approx -\frac{a_3}{a_1} o_2 \\ \frac{\partial o_2}{\partial t} &\approx \frac{a_4}{a_2} o_1. \end{aligned} \tag{11}$$

When we calculate the coefficients, either by finding the area under the curves in figure 6 or by directly calculating the correlations in the above equations using the CRH and MDC, and solve the system of equations we get an elliptical solution that matches the oscillation. We have not shown the scatter plot of the oscillation with the solution to the set of equations above because it is not informative and have instead opted for a more descriptive diagram in figure (8).

The state of the model at any given time is shown as the red dot and the oscillation is shown as the black ellipse. The two sets of axes are the basis formed by the two-mode model and the moisture variables plotted on top of each other. Visualizing both sets of axes is important because if we were to look only at the two-mode phase plane the tilted ellipse is puzzling, and by laying the moisture phase plane it becomes clear why it is aligned so. The moisture axis is shifted so that it is centered at the mean values that define our anomalies. The axis is rotated relative to the vertical motion axis because of the asymmetric nature of how the two modes interact with each other and the MSE budget.

We begin a period at point 1, with bottom-heavy lightly ascending air, high MDC, and low CRH. The column moistens throughout driving an increase in both modes moving the dot towards point 2. The vertical motion is deep and slightly top-heavy, the CRH is nearing its maximum and the MDC is starting to decrease. The first mode continues to effectively move MSE from the lower to upper troposphere while the second mode removes moisture from the lower troposphere, leading us around the curve as the second mode becomes stronger than the first and the CRH begins to decrease depositing us at point 3. The vertical motion at this point is stratiform and the moisture is primarily concentrated in the upper troposphere. The first mode becomes smaller and has less of an

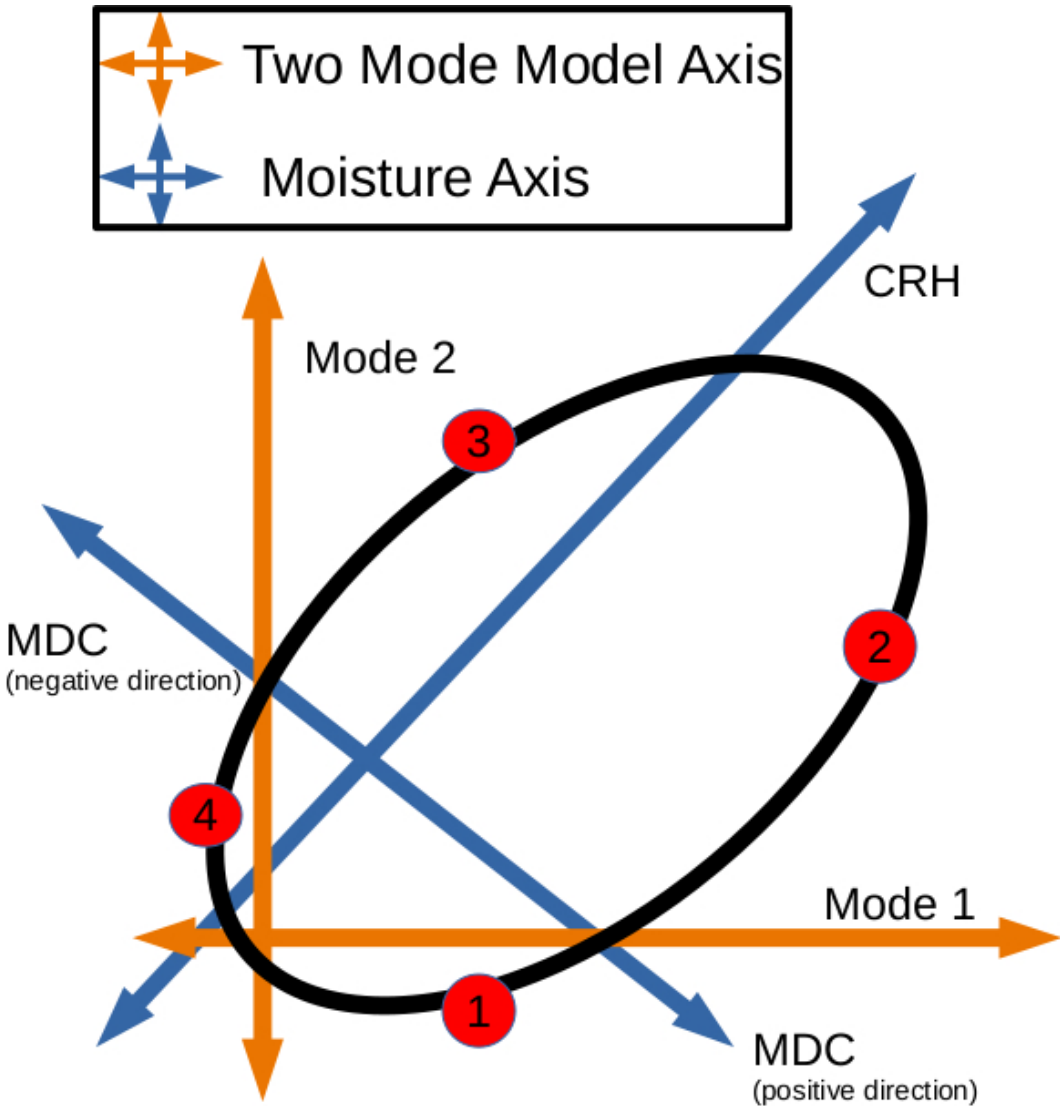

Figure 8. Schematic of the periodic oscillation, given in equation (11), viewed on two phase planes: the vertical motion phase plane and the moisture phase plane. The orange axis is for the two-mode model basis and the blue axis is for the moisture basis. The moisture axis is defined using the column humidity and the MDC, a measure of the moisture dipole, so that a decrease in MDC correlates with an increase in mode 2. The model state at any moment is shown as the red dot and the path that it takes during an oscillation is shown as the black line.

effect, while the second mode slowly removes moisture from the lower troposphere driving us to point 4 where the atmosphere is near its driest and the first mode becomes slightly negative which begins to increase the lower tropospheric moisture and decrease the upper tropospheric moisture, increasing the MDC. When the upper troposphere has dried enough the second mode becomes negative and begins to increase the lower tropospheric moisture and MDC even further catapulting the oscillation to begin the journey again at the start.

The two-mode model provides a qualitative description of our oscillation. In the next section, we will discuss the implications of the model and what conclusions may be drawn from our results.

5 Discussion

The periodic equilibrium has been seen in other research using the WTG approximation (Raymond et al. (2024), Wong and Kuang (2023), and personal correspondence with Dr. Tristan Abbott), although there are important differences between our setup and the other model setups which produced the periodic oscillation. Both Wong and Kuang (2023) and Raymond et al. (2024) observed the oscillation without interactive radiation. The former found the periodic equilibrium when the relaxation timescale was varied, during idealized modeling to compare WTG formulations. The latter found the periodic equilibrium during less idealized simulations of field campaign data. Dr. Tristan Abbott found the oscillation while using interactive radiation when the SST was increased by a small amount in idealized simulations. The variety of conditions and perturbations that bring about the oscillatory behavior is too broad and complex to have an obvious and simple solution and requires further investigation.

Some aspects of the periodic oscillation that we have described above are somewhat prevalent in the literature, although this has not been highlighted to this point. The oscillation that we describe here is similar to some aspects of the oscillatory behavior that is seen in Maithel and Back (2022) with both the moisture signature and effect of radiation and vertical advection contributing partially to driving the moisture recharge discharge cycles that the authors note. The periodic equilibrium meets the criteria for a moisture mode which means that it is also similar to a great deal of the variability which has been investigated (e.g. Jiang et al. (2018) and Mayta et al. (2022)). The real world is not temporally stationary like our model but a better understanding of the oscillations that the model generates will help us to understand what confines the oscillations to a particular shape and could help us better understand the evolution of convection (e.g. Wolding et al. (2022)).

The two-mode model acts as a kind of predator-prey system, with the two modes generating and consuming each other through the MSE anomalies captured by the CRH and MDC. This is a particularly attractive possibility because of the substantial mathematical foundation that exists to understand systems of this type. If we were able to obtain the coefficients in equation (7) *a priori*, we could determine which equilibrium the simulation would fall into before running the SWTG simulation.

The coefficients are also important because of their relation to how the moisture and two-mode axes are translated and rotated relative to each other and why the oscillation appears. They are a linearization of the functional relationship between the MSE and DSE budgets of moist convection. The functional relationship is moderated by factors like the radiation-moisture relationship, moisture-precipitation relationship, and fractional entrainment and detrainment rates. A better understanding of how these coefficients are determined and if they are predictable could shed light on better ways of parameterizing moist convection.

While the details of how the two axes are related would be helpful, the schematic diagram using them is still a good tool for understanding the oscillation and the multiple equilibria phenomena more generally. On the two-mode phase plane, both the moist and dry equilibrium states move towards a very particular equilibrium point and stay in the neighborhood of it while randomly jiggling around it. Taking the average over a long time highlights this equilibrium point and removes the random variability of the jiggling. The periodic equilibrium, on the other hand, settles into an elliptical orbit.

In this way, it is also good for showing how the oscillation, while a steady-state equilibrium, is fundamentally different from the other two equilibria because the mean behavior is not able to represent important variability. The time average of the periodic equilibrium will give a point inside of the orbit that the model state never actually reaches. This contrasts with the dry and moist equilibria which settle into a spot that defines the mean. This can be important when asking questions like "Do the radiation and vertical MSE advection balance?" In this oscillation, they balance if you ask the column-integrated MSE anomaly, but not if you ask the column-integrated MSE tendency at a given time.

6 Conclusion

We have discovered a new kind of WTG multiple equilibrium state which is characterized by a periodic oscillation in the vertical motion and moisture. This oscillatory state is a vertical motion moisture mode according to the criteria developed by Ahmed et al. (2021) and applied by Mayta et al. (2022). The moisture mode results from an environment that is laterally homogeneous and constant in time and is due to radiation and vertical advection and their interaction.

We can describe the vertical motion profile moisture mode as a closed elliptical loop on a set of axes defined by either a two-mode decomposition of the vertical motion or moisture. The vertical motion axis describes whether vertical motion is ascending or descending and top or bottom-heavy and comes from principal component analysis of a 40-year climatology of daily maritime vertical motion data from ERA5. The moisture axis is defined using the CRH and MDC because they capture the moisture variability related to the oscillation well. We can understand the ellipse by relating changes in each of the two axes to each other, with moisture variations driving vertical motion changes and vice versa. The oscillation acts as a sort of predator-prey dynamic between the moisture and vertical motion anomalies, forming a limit cycle on the phase planes of moisture and vertical motion. We can solve the set of equations and get a solution that qualitatively matches the oscillation.

The existence of the oscillation, and multiple equilibria, in WTG models is contingent on many particular factors. The large-scale temperature and initial moisture profiles, wind profiles, SST, and parameterizations of radiation and horizontal moisture transport are some of the factors that we found to be important to which equilibrium state the model settles into and the existence of the periodic oscillation. While we have provided a description of the oscillation and know many of the factors that control it, we do not have an explanation for its emergence. A deeper understanding of how the periodicity emerges from moist convective processes is needed to fully understand the oscillation. The existence of the periodic equilibrium and the potential for the advances in understanding that they can help with is fascinating and compelling.

Open Research Section

The data used in this study comes from simulations using WRF (v3.5.1) (Skamarock et al., 2008) and the WTG parameterization from (Wang et al., 2016). The model is initialized with ERA5 reanalysis data from the Copernicus Data Store (CDS) for both pressure levels (Hersbach et al., 2019b) and single levels (Hersbach et al., 2019c) on June 30,

2020. The scripts and simulation data used in the creation of the figures can be found at `https://github.com/mbernard3605//JAMES_WTG_periodic_equilibrium_data/` (Bernardez, 2024).

Acknowledgments
Thank you to Quinn Bowman for their constructive criticism and help developing this work. This work was supported by NSF Award #1759793 and the advanced opportunity fellowship at the University of Wisconsin.

References

Adames, Á. F. (2017). Precipitation budget of the Madden-Julian oscillation. *Journal of the Atmospheric Sciences*, *74*(6), 1799–1817. doi: 10.1175/JAS-D-16-0242.1

Adames, Á. F. (2022). The Basic Equations under Weak Temperature Gradient Balance: Formulation, Scaling, and Types of Convectively-coupled Motions. *Journal of the Atmospheric Sciences*, *79*(6), 2087–2108. doi: 10.1175/JAS-D-21-0215.1

Adames, Á. F., & Kim, D. (2016). The MJO as a dispersive, convectively coupled moisture wave: Theory and observations. *Journal of the Atmospheric Sciences*, *73*(3), 913–941. doi: 10.1175/JAS-D-15-0170.1

Adames, Á. F., Kim, D., Clark, S. K., Ming, Y., & Inoue, K. (2019). Scale analysis of moist thermodynamics in a simple model and the relationship between moisture modes and gravity waves. *Journal of the Atmospheric Sciences*, *76*(12), 3863–3881. doi: 10.1175/JAS-D-19-0121.1

Adames, A. F., & Maloney, E. D. (2021). Moisture mode theory's contribution to advances in our understanding of the madden-julian oscillation and other tropical disturbances. *Current Climate Change Reports*, *7*, 72–85.

Ahmed, F., David Neelin, J., & Adames, Á. F. (2021). Quasi-equilibrium and weak temperature gradient balances in an equatorial beta-plane model. *Journal of the Atmospheric Sciences*, *78*(1), 209–227. doi: 10.1175/JAS-D-20-0184.1

Andersen, J. A., & Kuang, Z. (2012). Moist static energy budget of MJO-like disturbances in the atmosphere of a zonally symmetric aquaplanet. *Journal of Climate*, *25*(8), 2782–2804. doi: 10.1175/JCLI-D-11-00168.1

Back, L. E., & Bretherton, C. S. (2009a). On the relationship between SST gradients, boundary layer winds, and convergence over the tropical oceans. *Journal of Climate*, *22*(15), 4182–4196. doi: 10.1175/2009JCLI2392.1

Back, L. E., & Bretherton, C. S. (2009b). A simple model of climatological rainfall and vertical motion patterns over the tropical oceans. *Journal of Climate*, *22*(23), 6477–6497. doi: 10.1175/2009JCLI2393.1

Back, L. E., Hansen, Z., & Handlos, Z. (2017). Estimating Vertical Motion Profile Top-Heaviness: Reanalysis Compared to Satellite-Based Observations and Stratiform Rain Fraction. *Journal of the Atmospheric Sciences*, *74*(3), 855–864. doi: 10.1175/jas-d-16-0062.1

Bernardez, M. (2024). *Data files and matlab scripts used for this paper* [software]. doi: https://doi.org/10.5281/zenodo.10946777

Bernardez, M., & Back, L. (2024). Integrating thermodynamic and dynamic views on the control of the top-heaviness of convection in the pacific itcz with weak temperature gradient simulations. *Journal of Advances in Modeling Earth Systems*, *16*(2), e2022MS003455.

Charney, J. G. (1963). A note on large-scale motions in the tropics. *Journal of the Atmospheric Sciences*, *20*(6), 607–609.

Chou, M.-D., & Suarez, M. J. (1999). *A solar radiation parameterization for atmospheric studies* (Tech. Rep.).

Fuchs, Ž., & Raymond, D. J. (2007, jan). A simple, vertically resolved model of tropical disturbances with a humidity closure. *Tellus A: Dynamic Meteorology and Oceanography*, *59*(3), 344–354. Retrieved from `https://www.tandfonline.com/doi/full/10.1111/j.1600-0870.2007.00230.x` doi: 10.1111/j.1600-0870.2007.00230.x

Herman, M. J., & Raymond, D. J. (2014). WTG cloud modeling with spectral decomposition of heating. *Journal of Advances in Modeling Earth Systems*, *6*(4), 1121–1140. doi: 10.1002/2014MS000359

Hersbach, H., Bell, P., B. Berrisford, Biavati, G., Horányi, A., Muñoz Sabater, J., Nicolas, J., ... Thépaut, J.-N. (2019a). *Era5 monthly averaged data on pressure levels from 1979 to present. copernicus climate change service (c3s) climate data store (cds).* (Accessed: 2019-06)

Hersbach, H., Bell, P., B. Berrisford, Biavati, G., Horányi, A., Muñoz Sabater, J., Nicolas, J., ... Thépaut, J.-N. (2019b). *Era5 monthly averaged data on pressure levels from 1979 to present. copernicus climate change service (c3s) climate data store (cds).* (Accessed: 2019-06) doi: 10.24381/cds.6860a573

Hersbach, H., Bell, P., B. Berrisford, Biavati, G., Horányi, A., Muñoz Sabater, J., Nicolas, J., ... Thépaut, J.-N. (2019c). *Era5 monthly averaged data on single levels from 1959 to present. copernicus climate change service (c3s) climate data store (cds).* (Accessed: 2019-06) doi: 10.24381/cds.f17050d7

Iacono, M. J., Delamere, J. S., Mlawer, E. J., Shephard, M. W., Clough, S. A., & Collins, W. D. (2008). Radiative forcing by long-lived greenhouse gases: Calculations with the aer radiative transfer models. *Journal of Geophysical Research: Atmospheres*, *113*(D13).

Inoue, K., Adames, Á. F., & Yasunaga, K. (2020). Vertical velocity profiles in convectively coupled equatorial waves and mjo: New diagnoses of vertical velocity profiles in the wavenumber–frequency domain. *Journal of the Atmospheric Sciences*, *77*(6), 2139–2162.

Jiang, X., Ángel F. Adames, Zhao, M., Waliser, D., & Maloney, E. (2018). A unified moisture mode framework for seasonality of the madden–julian oscillation. *Journal of Climate*, *31*(11), 4215 - 4224. Retrieved from `https://journals.ametsoc.org/view/journals/clim/31/11/jcli-d-17-0671.1.xml` doi: https://doi.org/10.1175/JCLI-D-17-0671.1

Klemp, J. B., Dudhia, J., & Hassiotis, A. D. (2008). An upper gravity-wave absorbing layer for nwp applications. *Monthly Weather Review*, *136*(10), 3987 - 4004. Retrieved from `https://journals.ametsoc.org/view/journals/mwre/136/10/2008mwr2596.1.xml` doi: https://doi.org/10.1175/2008MWR2596.1

Maithel, V., & Back, L. (2022). Moisture recharge–discharge cycles: A gross moist stability–based phase angle perspective. *Journal of the Atmospheric Sciences*, *79*(9), 2401 - 2417. Retrieved from `https://journals.ametsoc.org/view/journals/atsc/79/9/JAS-D-21-0297.1.xml` doi: https://doi.org/10.1175/JAS-D-21-0297.1

Mapes, B. E., Chung, E. S., Hannah, W. M., Masunaga, H., Wimmers, A. J., & Velden, C. S. (2018). The Meandering Margin of the Meteorological Moist Tropics. *Geophysical Research Letters*, *45*(2), 1177–1184. doi: 10.1002/2017GL076440

Matsui, T., Tao, W., & Shi, R. (2007). Goddard radiation and aerosol direct effect in goddard wrf. In *Nasa/umd wrf workshop.*

Mayta, V. C., Adames, Á. F., & Ahmed, F. (2022). Westward-Propagating Moisture Mode Over the Tropical Western Hemisphere. *Geophysical Research Letters*, *49*(6), 1–10. doi: 10.1029/2022GL097799

Morrison, H., Thompson, G., & Tatarskii, V. (2009). Impact of cloud microphysics on the development of trailing stratiform precipitation in a simulated squall line: Comparison of one-and two-moment schemes. *Monthly weather review*, *137*(3), 991–1007.

Neogi, S., & Singh, M. S. (2022). Understanding Changes in the Tropical Circulation under Global Warming Using a Cloud-Resolving Model and a Conceptual Model. *Journal of Climate*, *35*(18), 5855–5868. doi: 10.1175/JCLI-D-21-0854.1

North, G. R., Bell, T. L., Cahalan, R. F., & Moeng, F. J. (1982, jul). Sampling Errors in the Estimation of Empirical Orthogonal Functions. *Monthly Weather Review*, *110*(7), 699–706. Retrieved from `http://journals.ametsoc.org/doi/10.1175/1520-0493(1982)110%3C0699:SEITEO%3E2.0.CO;2` doi: 10.1175/1520-0493(1982)110⟨0699:SEITEO⟩2.0.CO;2

Ramage, C. S. (1971). *Monsoon meteorology*. New York: Academic Press.

Raymond, D. J., Fuchs, Ž., & Sentić, S. (2024). Rains and showers in otrec; weak temperature gradient modeling. *Journal of Advances in Modeling Earth Systems*.

Raymond, D. J., Sessions, S. L., Sobel, A. H., & Fuchs, Ž. (2009). The Mechanics of Gross Moist Stability. *Journal of Advances in Modeling Earth Systems*, *1*(3), n/a–n/a. doi: 10.3894/james.2009.1.9

Raymond, D. J., & Zeng, X. (2005). Modelling tropical atmospheric convection in the context of the weak temperature gradient approximation. *Quarterly Journal Of The Royal Meteorological Society*, *131*(608), 1301–1320. Retrieved from `http://doi.wiley.com/10.1256/qj.03.97%5Cnpapers2://publication/doi/10.1256/qj.03.97` doi: 10.1256/qj.03.97

Romps, D. M. (2021). Ascending columns, WTG, and convective aggregation. *Journal of the Atmospheric Sciences*, *78*(2), 497–508. doi: 10.1175/JAS-D-20-0041.1

Sentić, S., & Sessions, S. L. (2017, jun). Idealized modeling of convective organization with changing sea surface temperatures using multiple equilibria in weak temperature gradient simulations. *Journal of Advances in Modeling Earth Systems*, *9*(2), 1431–1449. Retrieved from `https://onlinelibrary.wiley.com/doi/10.1002/2016MS000873` doi: 10.1002/2016MS000873

Sessions, S. L., Herman, M. J., & Sentić, S. (2015). Convective response to changes in the thermodynamic environment in idealized weak temperature gradient simulations. *Journal of Advances in Modeling Earth Systems*, *7*, 712–738. doi: 10.1002/2013MS000282.Received

Sessions, S. L., Sentic, S., & Herman, M. J. (2016). The role of radiation in organizing convection in weak temperature gradient simulations. *Journal of Advances in Modeling Earth Systems*, *8*(1), 244–271. doi: 10.1002/2015MS000587

Sessions, S. L., Sugaya, S., Raymond, D. J., & Sobel, A. H. (2010). Multiple equilibria in a cloud-resolving model using the weak temperature gradient approximation. *Journal of Geophysical Research*, *115*, D12110. Retrieved from `http://www.agu.org/pubs/crossref/2010/2009JD013376.shtml` doi: 10.1029/2009JD013376

Shi, J. J., Tao, W.-K., Matsui, T., Cifelli, R., Hou, A., Lang, S., ... others (2010). Wrf simulations of the 20–22 january 2007 snow events over eastern canada: Comparison with in situ and satellite observations. *Journal of Applied Meteorology and Climatology*, *49*(11), 2246–2266.

Singh, M. S., & Neogi, S. (2022). On the Interaction between Moist Convection and Large-Scale Ascent in the Tropics. *Journal of Climate*, *35*(14), 4417–4435. doi: 10.1175/JCLI-D-21-0717.1

Singh, M. S., Warren, R. A., & Jakob, C. (2019). A Steady-State Model for the Relationship Between Humidity, Instability, and Precipitation in the Tropics. *Journal of Advances in Modeling Earth Systems*, *11*(12), 3973–3994. doi: 10.1029/2019MS001686

Skamarock, W. C., Klemp, J. B., Dudhia, J., Gill, D. O., Barker, D. M., Duda, M. G., ... Powers, J. G. (2008). *A Description of the Advanced Research WRF Version 3* (Tech. Rep.). University Corporation for Atmospheric Research.

(Note NCAR/TN-468+ STR) doi: http://dx.doi.org/10.5065/D68S4MVH

Sobel, A. H., Bellon, G., & Bacmeister, J. (2007). Multiple equilibria in a single-column model of the tropical atmosphere. *Geophysical Research Letters*, *34*(22), 1–5. doi: 10.1029/2007GL031320

Sobel, A. H., & Bretherton, C. S. (2000). Modeling tropical precipitation in a single column. *Journal of Climate*, *13*(24), 4378–4392. doi: 10.1175/1520-0442(2000)013⟨4378:MTPIAS⟩2.0.CO;2

Sobel, A. H., & Maloney, E. (2012). An idealized semi-empirical framework for modeling the madden–julian oscillation. *Journal of the Atmospheric Sciences*, *69*(5), 1691–1705.

Sobel, A. H., & Maloney, E. (2013). Moisture modes and the eastward propagation of the mjo. *Journal of the Atmospheric Sciences*, *70*(1), 187–192.

Sobel, A. H., Nilsson, J., & Polvani, L. M. (2001). The Weak Temperature Gradient Approximation and Balanced Tropical Moisture Waves*. *Journal of the Atmospheric Sciences*, *58*(23), 3650–3665. doi: 10.1175/1520-0469(2001)058⟨3650:TWTGAA⟩2.0.CO;2

Wang, S., Sobel, A. H., & Nie, J. (2016). Modeling the MJO in a cloud-resolving model with parameterized large-scale dynamics: Vertical structure, radiation, and horizontal advection of dry air. *Journal of Advances in Modeling Earth Systems*, *8*(1), 121–139. doi: 10.1002/2015MS000529

Wolding, B., Powell, S. W., Ahmed, F., Dias, J., Gehne, M., Kiladis, G., & Neelin, J. D. (2022). Tropical Thermodynamic-Convection Coupling in Observations and Reanalyses. *Journal of the Atmospheric Sciences*, *79*(6), 1781–1803. doi: 10.1175/JAS-D-21-0256.1

Wong, N. Z., & Kuang, Z. (2023). The effect of different implementations of the weak temperature gradient approximation in cloud resolving models. *Authorea Preprints*.